Regional Studies in Marine Science 93 (2026) 104691

Contents lists available at ScienceDirect

Regional Studies in Marine Science

journal homepage: www.elsevier.com/locate/rsma

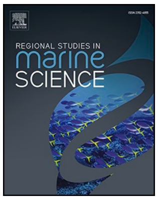

Numerical analysis of rip currents at RK Beach, Visakhapatnam, India using XBeach model

Sivaiah B[a,e,*], Surisetty V.V. Arun Kumar[b], Muhammad Zahir Ramli[c], Mohd Shahrizal Ab Razak[d], K. Siva Srinivas[a], Pottapinjara V[a], T. Sridevi[b], Rashmi Sharma[b], B. Ajay Kumar[a], V. Raam Balaji[a], P.S.N. Acharyulu[a], K. Venkateswara Rao[a,e], R. Harikumar[a], T.M. Balakrishnan Nair[a], Sudheer Joseph[a], B. Gireesh[e], Ch Venkateswarlu[e], C.V. Naidu[e]

[a] Indian National Centre for Ocean Information Services (INCOIS), Hyderabad, India
[b] Space Applications Centre (SAC), Ahmedabad, Gujarat, India
[c] Institute of Oceanography and Maritime Studies (INOCEM), Kuliyyah of Science, International Islamic University Malaysia, Kuantan, Pahang, Malaysia
[d] Department of Civil Engineering, Faculty of Engineering, Universiti Putra Malaysia, Serdang, Selangor, Malaysia
[e] Department of Meteorology and Oceanography, Andhra University, Visakhapatnam, India

ARTICLE INFO

Keywords:
XBeach
Rip currents
RK beach
Numerical modelling
Drifters
And satellite images

ABSTRACT

Rip currents are powerful, narrow currents that flow from the shore out to sea, originating within the surf zone due to the intricate interplay of waves, tides, currents, and the nearshore bathymetry. These currents pose significant danger, swiftly transporting swimmers and surfers offshore, resulting in numerous drownings globally. RK Beach in Visakhapatnam has reported a high number of rip current related drowning incidents. This study uses the 2D hydrostatic, phase-averaged, surf beat non-stationary mode of the XBeach model to simulate rip currents under diverse wave and tidal conditions. The primary inputs for the model consist of surveyed beach profile, nearshore bathymetry, wave fields from a nearby offshore wave rider buoy, and water levels from a tide gauge. Under nearly shore-normal wave incidence, particularly during the pre- and post-monsoon periods, intense velocities ranging from 0.5 to ~1.2 m/s were observed in the rip neck region, gradually decreasing toward the rip head. The model simulated rip current locations closely match the channels depicted in nearshore bathymetry, a pattern also observed in high-resolution satellite images, suggesting bathymetrically controlled rip currents. Model simulations conducted under diverse seasonal hydrodynamic conditions showed close agreement with field observations, indicating high model reliability in simulating rip current dynamics, with RMSE values of 0.1 m for significant wave height, 0.03 m for water level, 5–10° for peak wave direction, and 0.15 m/s for current velocity. This is further supported by the strong agreement between the modelled patterns and the observed drifter velocities, Rhodamine-B dye dispersion, dimensionless fall velocity parameter (Ω) and satellite imagery. This study provides a basis for future simulations with variable nearshore bathymetry derived from satellite or video sources and accurately predicted hydrodynamics from suitable nearshore models toward developing an operational rip current forecasting framework.

1. Introduction

Rip currents are intense, narrow water flows that transport water from the shore to offshore regions, typically forming in the surf zone due to alongshore variations in wave height and resultant radiation stress (Bowen and Douglas Inman, 1969; Longuet-Higgins and Stewart, 1964). These variations generate diverse circulation patterns, ranging from stable closed-loop systems to strong offshore-directed jets extending beyond the surf zone. Rip currents are a leading cause of drowning worldwide and are responsible for thousands of rescues every year (Brander, 2015; Surisetty and Prasad, 2014; Lushine, 1991). These currents pose a serious risk to beachgoers, as they can quickly drag swimmers of all skill levels out to deeper waters, leading to panic and exhaustion that often results in fatalities (Brander and MacMahan, 2011; Drozdzewski et al., 2012; Drozdzewski et al., 2015). These currents can reach velocities of 0.3–1 m/s and, under certain conditions, may exceed

---

* Corresponding author at: Indian National Centre for Ocean Information Services (INCOIS), Hyderabad, India.
E-mail addresses: siva4ocean@gmail.com, s.borra-p@incois.gov.in (S. B).

https://doi.org/10.1016/j.rsma.2025.104691
Received 20 May 2025; Received in revised form 19 October 2025; Accepted 4 December 2025

2.5 m/s (B. (Castelle et al., 2016); (MacMahan et al., 2006). Rip currents are often short-lived but can persist for minutes to hours or days or even months, depending on environmental conditions (Lippmann and Holman, 1989; Sasaki and Horikawa, 1978). Their movement and structure are strongly influenced by wave height, water levels, coastal bathymetry, and prevailing currents, making their behavior complex and difficult to predict (Brander and MacMahan, 2011).

The foundational theory of rip current dynamics, initially described by Longuet-Higgins, Stewart (Longuet-Higgins and Stewart, 1964), links their formation to variations in wave forcing caused by changes in wave height and the distribution of radiation stress. Bowen, Douglas Inman (Bowen and Douglas Inman, 1969) expanded on this, proposing that alongshore variations in wave forcing generate offshore-directed flows. Dalrymple and Lozano, (Dalrymple and Lozano, 1978) further advanced the theory, suggesting that rip currents are sustained through wave-current interactions, where incoming waves refract towards the currents, altering alongshore radiation stress and driving offshore circulation. Subsequent studies have confirmed that rip currents can develop due to spatial variations in onshore-directed wave forces, independent of external influences such as edge waves or pre-existing wave-current interactions (Caballeria et al., 2002; Kennedy and Zhang, 2008; Long and Özkan-Haller, 2016; Suanda and Feddersen, 2015; Yu and Slinn, 2003). These findings challenge earlier models that focused primarily on wave-driven flows, with more recent work by Long and Özkan-Haller, (Long and Özkan-Haller, 2016), (Castelle et al., 2016), and (Houser et al., 2011) emphasizing the role of alongshore variations in onshore wave forces as the primary mechanism for rip current generation.

Recent advancements in rip-current modeling include high-resolution simulations and hazard tools. XBeach is widely used for simulating nearshore dynamics, swimmer escape strategies (McCarroll et al., 2015), coastal dynamics (Castelle et al., 2014), swimmer safety (Sembiring et al., 2016), and for rip-current and shore-break hazard forecasting (Castelle et al., 2014). Other models, such as SWAN (Kumar et al., 2011) and FUNWAVE (Choi and Roh, 2021; Ji et al., 2023; Ji et al., 2025; Yuan et al., 2023), porous media models (Ji et al., 2025; Ji et al., 2025) are applied for wave dynamics and rip-current interactions. Delft3D (Reniers et al., 2010) models rip currents and coastal processes in detailed 3D settings, while NOAA's hazard model (Casper et al., 2024) provides real-time hazard predictions. These models collectively enhance rip-current safety and hazard prediction.

To reduce the risks associated with rip currents and improve coastal safety and recreational management, it is important to predict their occurrence and variability accurately. Numerical modeling serves as an effective approach to simulate rip current dynamics and their response to changing hydrodynamic conditions. To investigate rip current dynamics in the surf zone, this study used the XBeach model, which was originally developed by Deltares and Delft University of Technology in the Netherlands to simulate beach responses to extreme storm conditions (McCarroll et al., 2015). The model has been extensively applied to examine hydrodynamic processes within the surf zone, including wave propagation, currents, sediment transport, and bed changes (Scott et al., 2016). Its unsteady, directionally resolved wave driver captures the collective motion of wave groups critical for rip current generation (MacMahan et al., 2004). XBeach surpasses conventional phase-averaged models by resolving infragravity (IG) motions and low-frequency vortical currents induced by wave groups (Yuan et al., 2023), while incorporating wave breaking, radiation stress, and variable coastal bathymetry. The 2D, hydrostatic, phase-averaged surf-beat mode has been extensively validated for simulating surf-zone circulation and rip currents across diverse coastal settings (Castelle et al., 2014; McCarroll et al., 2015; Roelvink et al., 2009; Vousdoukas et al., 2011). The hydrostatic approximation remains appropriate for shallow surf zones where non-hydrostatic effects are secondary (MacMahan et al., 2006). Leveraging this established reliability, the present study applies the XBeach model at RK Beach to examine rip current variability under different wave and tidal conditions and to support the development of an operational forecasting framework. The compilation of rip current drowning incidents at major recreational beaches in Visakhapatnam, as presented in Table 1, was derived from multiple sources, including the concerned local police stations that maintain records of such incidents, published research articles, collaborations with organizations such as Reliance Foundation and Matsyakara Samkshema Samiti (MSS), and reports from prominent national and regional media outlets such as The Hindu and The Times of India. Among all the beaches, RK Beach in Visakhapatnam has been the most severely affected by rip current-related fatalities (Surisetty and Prasad, 2014; Surisetty et al., 2023). This alarming statistic underscores the need for effective rip current forecasting in the area. To address this, the study uses the XBeach model, the first of its kind in India for studying rip currents, to simulate and validate field-observed rip currents and their behavior under varying wave and tidal/water level conditions across seasons, with the aim of developing an operational forecast system capable of issuing timely alerts to lifeguards, enhancing beach safety, and reducing drowning risks.

2. Materials and methods

2.1. Study area

Ramakrishna Beach (hereafter RK Beach) in Visakhapatnam is a well-known coastal stretch along the eastern seaboard of India, extending approximately 2.5–3.0 km in a northeast-southwest direction, as depicted in Fig. 1. It features sandy shores, dunes, and wave-cut platforms (Raju and Vaidyanadhan, 1978). The beach has a steep foreshore with sand grains between 0.45 and 0.5 mm (Surisetty, 2012) and experiences semidiurnal tides with spring and neap ranges of 1.43 m and 0.54 m, respectively (Kumar et al., 2001). Alongshore currents flow northeast from March to September and southwest from November to February, with speeds ranging from 0.02 to 0.3 m per second (Kumar et al., 2006). Waves approach from the southeast during monsoon months and from the east to southeast in other seasons (Kumar et al., 2001; Kumar et al., 2004; Reddy et al., 1984). The region receives an annual rainfall of about 975 mm, influenced by the Indian Monsoon. Littoral drift transports 0.5–0.7 million cubic meters of sand per year toward the northeast (Kumar et al., 2001; Panigrahi et al., 2010). Strong hydrodynamic forces cause erosion and hazardous rip currents, making RK Beach the most dangerous in Visakhapatnam, with more than 500 rip current-related fatalities since 2006 (Sivaiah B. et al., 2022; Surisetty et al., 2023).

2.2. Field data

Field data were collected during field surveys conducted at RK Beach on May 15 and October 25, 2018. The data included drifter velocities and rhodamine B dye trajectories, which provided detailed observations of rip current behavior and offshore flow patterns (Surisetty et al., 2021). These observations were essential for validating the performance of the XBeach model. Additionally, satellite imagery from Google Earth (0.5–1.0 m) and Sentinel-2 (10 m), acquired near the fieldwork period, offered complementary insights by capturing rip channel features through gaps in wave breaking patterns. The collected data on rip current-related drownings at major beaches in Visakhapatnam indicate an increasing trend, particularly during the decade from 2010 to 2020, with the majority of incidents reported at RK Beach, Rushikonda, Yarada, Bheemili, and Jodugullapalem, followed by other beaches, as shown in Table 1. A total of 529 incidents were recorded from 2000 to 2023, however additional drowning cases may have gone unreported.

Wave and water level data for the entire year 2018 were obtained from a nearby coastal wave rider buoy and a tide gauge station operated by INCOIS (Indian National Centre for Ocean Information Services, https://www.incois.gov.in). The year-round data were plotted to

Table 1
Annual number of rip current-related drowning incidents reported at different beaches in Visakhapatnam from 2000 to 2023.

Year	RK Beach	Rushikonda Beach	Yarada Beach	Bheemili Beach	Jodugulla Palem Beach	Sagar Nagar Beach	Other Beaches	Total
2000	4	9	3	1	2	1	3	23
2001	10	10	3	2	1	0	1	27
2002	8	3	0	0	0	2	2	15
2003	4	2	1	2	3	0	2	14
2004	2	1	1	0	1	1	1	07
2005	13	5	1	5	0	0	2	26
2006	4	6	3	3	0	0	0	16
2007	13	3	3	0	0	1	3	23
2008	18	2	1	2	1	2	4	30
2009	10	4	4	0	3	1	6	28
2010	7	8	3	4	4	0	1	27
2011	15	5	7	1	0	0	4	32
2012	4	12	3	3	3	2	3	30
2013	10	0	1	0	1	0	7	19
2014	11	2	4	0	2	0	2	21
2015	12	1	1	1	1	0	2	18
2016	14	2	5	3	2	1	6	33
2017	12	3	4	3	1	2	7	32
2018	7	2	0	4	1	1	2	17
2019	6	3	1	5	0	0	1	16
2020	0	0	4	7	0	1	3	15
2021	15	1	1	5	0	1	2	25
2022	9	6	0	4	0	0	7	26
2023	3	2	1	2	0	0	2	10
Total	**211**	**92**	**56**	**55**	**26**	**16**	**73**	**529**

illustrate overall variations, with subplots highlighting the conditions during the field experiments conducted on May 15 and October 25, 2018, as shown in Fig. 2. The wave rider buoy provided critical parameters, including significant wave height, peak wave period, and direction, while the tide gauge recorded water level variations. The model simulations were validated against observational data to assess their accuracy and suitability as wave and tidal boundary inputs for rip current simulations using the XBeach model.

2.3. Beach topography and bathymetry:

The model computational domain, shown in Fig. 3, covers an area of approximately 2000 × 2000 m, with depths ranging from −21 m to 9 m. The computational grid has a varying mesh in the cross-shore direction, ranging from ~20 m at the offshore boundary to ~2 m near the shoreline, while a ~5–7 m grid size is used in the alongshore direction. High-resolution bathymetric data (~2–3 m) was obtained from a single-beam echosounder and merged with datasets from INCOIS, National Institute of Ocean Technology (NIOT https://www.niot.res.in) including toposheets, General Bathymetric Chart of the Oceans (GEBCO - https://www.gebco.net), and other sources.

Surveyed beach profiles were merged with topographic data using triangular interpolation, and the shoreline was digitized from a Google Earth images dated May 15 and 25 October, 2018. The bathymetry shows significant spatial variability, including deep channels and sandbars, including distinct sandbar-channel features, as depicted in Fig. 3. Bed level data for the model were derived from combined bathymetric and topographic survey data collected nearest to the simulation time of interest.

2.4. Numerical model

In numerical modelling, the wave-induced momentum is represented through radiation stress, which accounts for the depth-integrated flux of momentum due to waves. As waves approach the shore, they exert momentum transport, termed radiation stress. The spatial variation of this stress generates a wave-induced force, which can be expressed as:

$$F_x = \frac{\partial S_{xx}}{\partial x} \tag{1}$$

where S_{xx} [N·m^{-2}] denotes the cross-shore component of radiation stress, and F_x [N·m^{-3}] represents the wave-induced force per unit volume. For a steady-state momentum balance, this wave-induced force is counteracted by the hydrostatic pressure gradient, which causes set-up and set-down of the water surface, represented as:

$$F_x = -\rho g(h+\eta)\frac{\partial \eta}{\partial x} \tag{2}$$

where h[m] is the still-water depth, η[m] is the free surface elevation, and ρ[kg·m^{-3}] and g[m·s^{-2}] denote the water density and gravitational acceleration, respectively. When both cross-shore (x) and alongshore (y) components are considered, the momentum balance equations include the combined effects of radiation stress and hydrostatic forces as:

$$F_x = -\frac{\partial S_{xx}}{\partial x} - \rho g(h+\eta)\frac{\partial \eta}{\partial x} \tag{3}$$

$$F_y = -\frac{\partial S_{yy}}{\partial y} - \rho g(h+\eta)\frac{\partial \eta}{\partial y} \tag{4}$$

These relationships describe how spatial variations in radiation stress and hydrostatic pressure gradients interact to drive nearshore circulation, leading to phenomena such as wave setup, longshore currents, and rip current formation, and their variability across different coastal settings.

The XBeach model (Roelvink et al., 2009) is a computational framework designed to simulate wave behavior, nearshore currents, and sediment transport on sandy coasts over spatial scales of kilometers and temporal scales of storm events. The model solves coupled two-dimensional (2D) horizontal equations for wave propagation, currents, sediment transport, and bed variation, considering varying spectral wave and flow boundary conditions. It governs wave action, mass, and momentum, facilitating interactions between waves and currents (Dudkowska et al., 2020), while applying depth-averaged Generalized Lagrangian Mean (GLM) formulations of the shallow water equations to compute wave-induced mass flux and return flow (Roelvink et al., 2010).

The shallow water momentum equations in the XBeach model are expressed in two directions: cross-shore (x) and alongshore (y). The

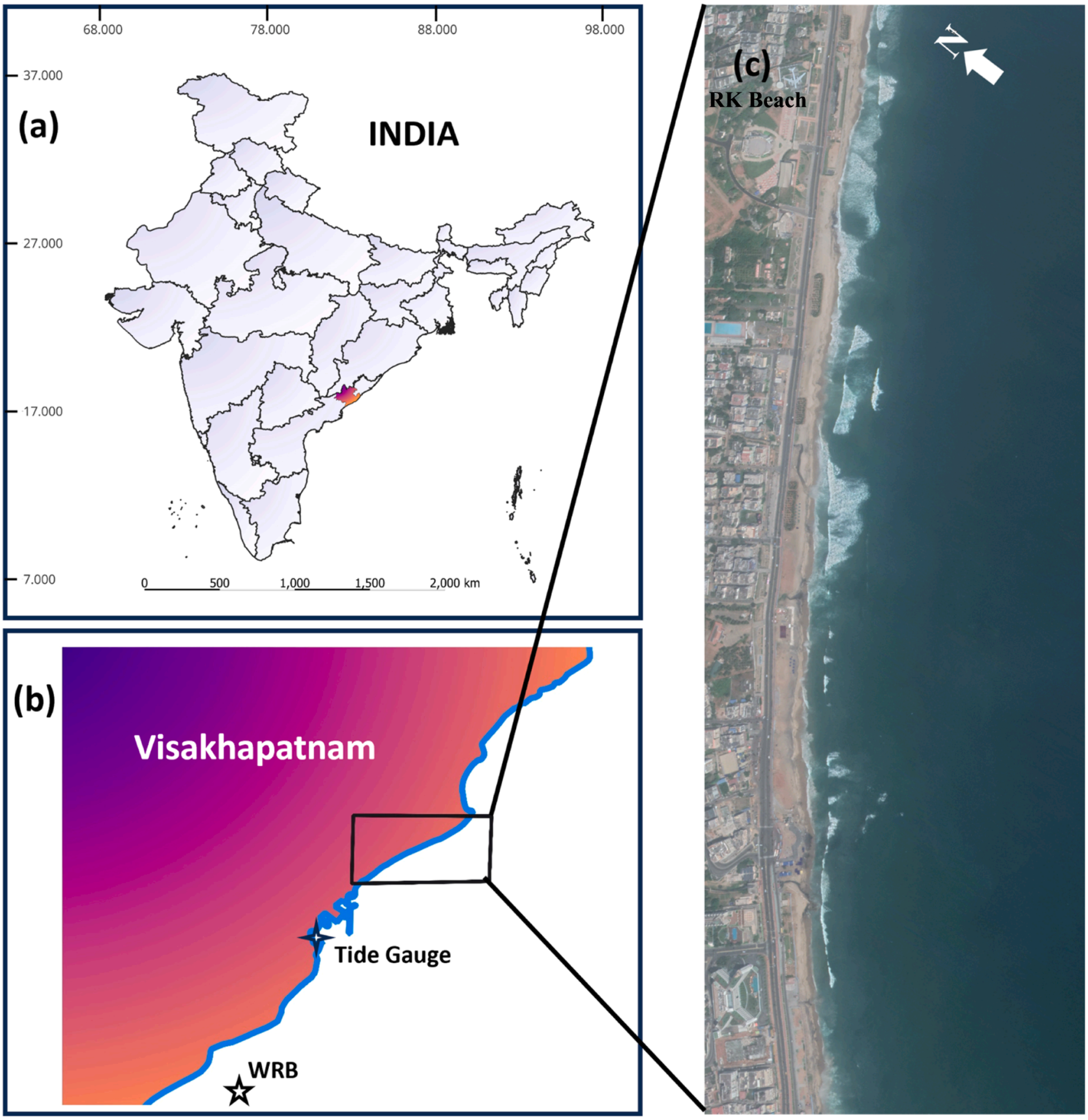

Fig. 1. (a). India location map, (b). Coastal stretch of Visakhapatnam, (c). RK Beach - satellite image sourced from Google Earth, acquired on 2018–10–27.

equations governing the flow dynamics are as follows:

Momentum equation in the x-direction:

$$\frac{\partial u}{\partial t}+u\frac{\partial u}{\partial x}+v\frac{\partial u}{\partial y}-fv-\nu_h\left(\frac{\partial^2 u}{\partial x^2}+\frac{\partial^2 u}{\partial y^2}\right)=\frac{\tau_{wx}}{\rho h}-\frac{\tau_{bx}}{\rho h}-g\frac{\partial \eta}{\partial x}+\frac{F_x}{\rho h} \tag{5}$$

Momentum equation in the y-direction:

$$\frac{\partial v}{\partial t}+u\frac{\partial v}{\partial x}+v\frac{\partial v}{\partial y}+fu-\nu_h\left(\frac{\partial^2 v}{\partial x^2}+\frac{\partial^2 v}{\partial y^2}\right)=\frac{\tau_{wy}}{\rho h}-\frac{\tau_{by}}{\rho h}-g\frac{\partial \eta}{\partial y}+\frac{F_y}{\rho h} \tag{6}$$

Mass continuity equation:

$$\frac{\partial \eta}{\partial t}+\frac{\partial (hu)}{\partial x}+\frac{\partial (hv)}{\partial y}=0 \tag{7}$$

where $\tau_{wx}=\rho_a c_d|W|W_x$ sand $\tau_{wy}=\rho_a c_d|W|W_y$.

Here, τ_{wx},τ_{wy}[N·m^{-2}] are the wind shear stresses, ρ_a[kg·m^{-3}] is the air density, $c_d$is the wind drag coefficient, and W[m·s^{-1}] is the wind velocity. τ_{bx},τ_{by}[N·m^{-2}] are the bed shear stresses, η[m] is the water level, F_x,F_y[N·m^{-2}] are the wave-induced stresses, f[s^{-1}] is the Coriolis coefficient, ν_h[m^2·s^{-1}] is the horizontal eddy viscosity, and h[m] is the water depth relative to mean sea level.

The radiation stresses are derived from the wave action equation for short waves, expressed as:

$$\frac{\partial A}{\partial t}+\frac{\partial (C_xA)}{\partial x}+\frac{\partial (C_yA)}{\partial y}+\frac{\partial (C_\theta A)}{\partial \theta}=\frac{D_w}{\sigma} \tag{8}$$

where A is the wave action, σ[s^{-1}] is the intrinsic wave frequency, θ[radians] is the angle of wave incidence with respect to the x-axis, C_x, C_y[m·s^{-1}] and C_θ[rad·s^{-1}] are the wave action propagation speeds in the x, y, and θ directions, respectively, and D_w[W·m^{-2}] is the total wave dissipation in each directional bin.

The simulations were carried out using the XBeach model (version 1.23.5526 XBeachX release) in surfbeat mode, which employs a nonstationary, directionally spread wave driver to resolve short-wave energy variations at the group scale and accurately represent wave group induced motions that are critical for rip current dynamics (MacMahan et al., 2004). Offshore boundary conditions for the XBeach model were derived from directional wave rider buoy data recorded every 30 min at a depth of 20 m offshore of Visakhapatnam, including significant wave height, peak wave period, and wave direction, along

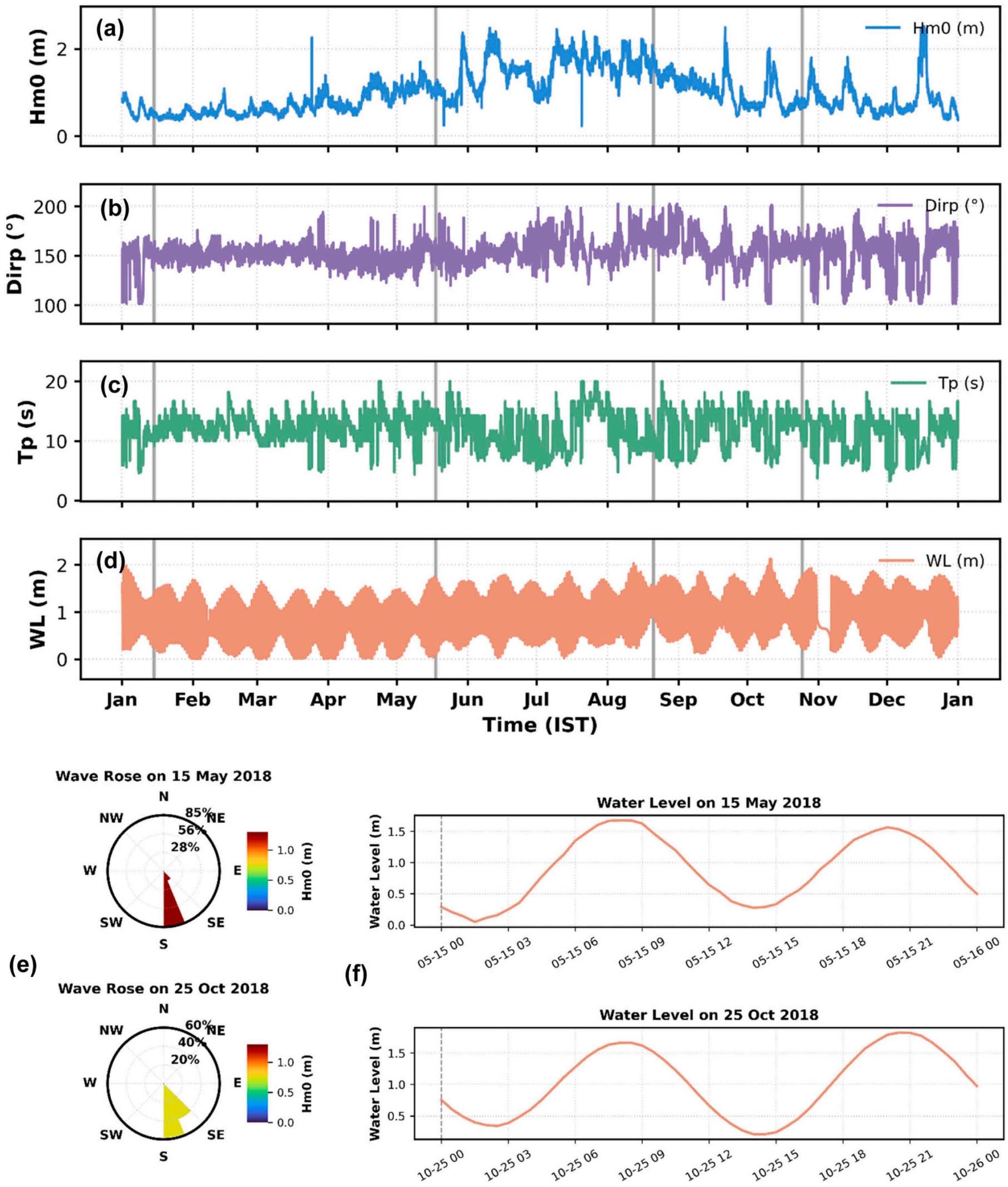

Fig. 2. Wave rider buoy and tide gauge observations during 2018 showing (a) significant wave height, (b) peak wave direction, (c) peak wave period, and (d) water level for the full year. (e) Wave roses and (f) water levels correspond to the survey periods on 15 May and 25 October 2018, respectively. Shaded bars in (a-d) denote the simulation dates: 15 January, 15 May, 21 August, and 25 October 2018.

with water level data from the nearby INCOIS tide gauge station. Bed friction was represented using the Chezy formulation, and sensitivity experiments were conducted with Chezy coefficients ranging from 20 to 40, where a value of 35 produced the most stable and realistic results. The sediment grain size (D_{50}) in the study area ranged from 0.18 to 0.9 mm, indicating a relatively uniform sandy composition. The model was initialized from rest and executed for four representative periods, January 15, May 15, August 21, and October 25, 2018, to capture seasonal hydrodynamic conditions. For each simulation, the first hour was treated as a spin-up period and excluded from analysis to ensure model stability before evaluation.

2.5. Beach morphodynamic classification and rip current risk assessment

Coastal morphodynamics are primarily governed by the interaction between incident wave energy, sediment characteristics, and beach slope, which together determine the dynamic equilibrium of beach states (Masselink and Short, 1993; Short, 2006). The dimensionless fall velocity parameter (Ω) proposed by Wright and Short (Wright and Short, 1984) is a widely used morphodynamic index that represents the balance between wave forcing and sediment settling response and is defined as:

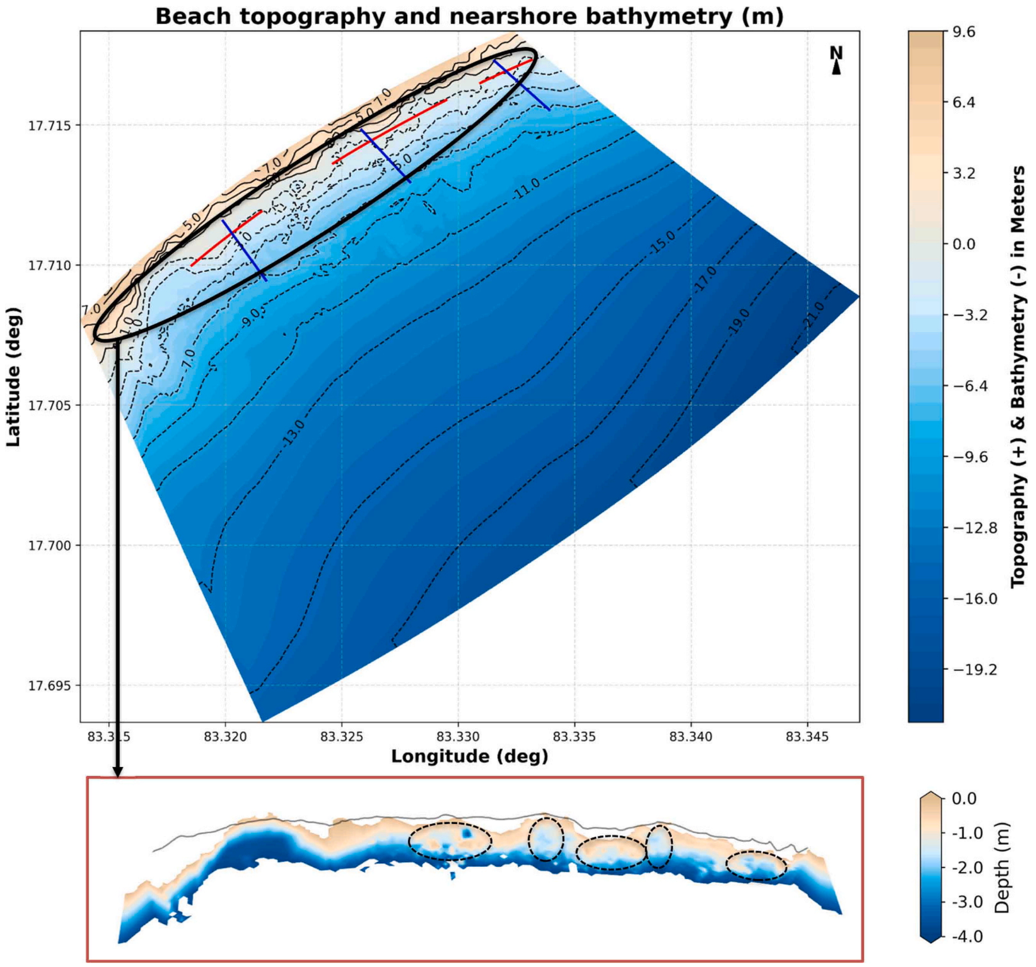

Fig. 3. Beach topography and nearshore bathymetry of the study area showing elevation and depth variations. Black contours represent topographic and bathymetric features, while red and blue transects indicate cross-shore and longshore sections used for analysis. The outlined black oval marks the detailed surf zone (0 to −4 m depth), illustrating distinct sandbars and channels.

$$\Omega = \frac{H_b}{TW_s} \tag{9}$$

where H_b is the breaker wave height (m), T is the wave period (s), and W_s is the sediment fall velocity (m s^{-1}). This parameter quantitatively classifies beaches into reflective, intermediate, and dissipative states. Higher Ω values indicate stronger wave energy relative to sediment settling, resulting in wide, dissipative beaches, while smaller Ω values represent reflective beaches with steeper profiles and coarse sediments.

The breaker height (H_b) was estimated from offshore significant wave height (H_∞) and period (T) using the empirical relationship of Komar, Gaughan (Komar and Gaughan, 1973),

$$H_b = 0.39g^{1/5}\left(TH_\infty^2\right)^{2/5} \tag{10}$$

where gis the gravitational acceleration (9.81 m s^{-2}). The sediment fall velocity (W_s) was computed using the Ferguson and Church (Ferguson and Church, 2004) formulation,

$$W_s = \frac{RgD^2}{C_1\nu + \sqrt{0.75C_2RgD^3}} \tag{11}$$

where R is the submerged specific gravity of sediment (≈ 1.65), D is the median grain size (D_{50}, m), ν is the kinematic viscosity of seawater (≈ 1×10^{-6} m^2 s^{-1}), and $C_1 = 24$, $C_2 = 1.2$. This formulation effectively captures both viscous and turbulent settling regimes, providing reliable estimates of sediment behavior under natural beach conditions (Dean and Robert, 2004). The Ω parameter also serves as an indicator of rip-current susceptibility, where intermediate beach states, such as Low-Tide Terrace (LTT), Rhythmic Bar and Beach (RBB), and Transverse Bar and Rip (TBR), are known to support stronger and more persistent rip currents compared to reflective (R) or dissipative (D) conditions (Short and Brander, 1999; Wright and Short, 1984), as shown in Table 2.

3. Results

3.1. Model simulations under seasonal hydrodynamics:

The model was run for four representative periods, January 15, May 18, August 21, and October 25, 2018, to capture seasonal variability in nearshore hydrodynamics along the study stretch. Each simulation covered a full tidal cycle, including both flood and ebb phases, to assess temporal and spatial variations in significant wave height (SWH), water level (Zs), and current velocity fields, with focus on rip current formation and circulation patterns. Among these, simulations for May 15 and October 25 were analyzed in detail owing to the availability of concurrent field observations.

The simulated SWH, water level, and current vectors overlaid on current magnitude for May 15, 2018, as shown in Fig. 4, correspond to 01:30, 08:10, and 14:10 Indian Standard Time (IST), representing low, high, and subsequent low tide phases. The SWH ranged from 0.3 to 2.2 m, indicating energetic pre-monsoon conditions. During low tide (01:30 and 14:10), enhanced breaking and dissipation occurred near the

Table 2
Typical classification of beach morphodynamic states showing corresponding Ω ranges, characteristic beach features, and relative rip current likelihood (Short, 2006; Wright and Short, 1984).

Ω Range	Beach Morphodynamic Classification	Beach Characteristics	Rip current likelihood
$\Omega < 1$	Reflective (R)	Steep, narrow beach; coarse sediment; surging breakers; minimal surf zone	Very low
$1 \le \Omega < 3$	Intermediate Low-Tide Terrace (LTT)	Gently sloping beach; weak inner bar and terrace; moderate wave energy	Moderate
$3 \le \Omega < 5$	Intermediate Rhythmic Bar and Beach (RBB)	Alternating bar-trough formations; rhythmic breaker zones	High
$5 \le \Omega < 6$	Intermediate Transverse Bar and Rip (TBR)	Pronounced transverse bars and rip channels, plunging breakers	Very high
$6 \le \Omega < 7$	Intermediate Longshore Bar and Trough (LBT)	Continuous longshore bar; wide surf zone	Moderate to low
$\Omega \ge 7$	Dissipative (D)	Flat, wide beach; fine sediment; spilling breakers	Very low

shore, producing strong SWH gradients across the surf zone. At high tide (08:10), reduced breaking in deeper water allowed higher waves (up to 2.0 m) to propagate shoreward. The corresponding current fields revealed narrow, well-defined rips with greater offshore extent (0.8–1.5 m/s) during low tide, concentrated near morphological depressions, highlighted by dotted boxes, while high tide currents were mainly longshore-directed and weaker (0.4–0.8 m/s). Water levels varied between 0.4 and 1.9 m, with pronounced setup gradients nearshore driving strong cross-shore return flows. These results show that rip currents were more organized and intense during ebb phases, consistent with field observations under moderate to high wave energy.

Under post-monsoon conditions (October 25, 2018), the model simulated nearshore hydrodynamics over a full tidal cycle, with SWH, Zs, and current vectors extracted at 03:30, 09:30, and 15:30 IST, corresponding to low, high, and subsequent low tide, as illustrated in Fig. 5. The SWH ranged from 0.2 to 1.2 m, exhibiting clear spatial variability and gradual dissipation toward the shore. During low tide phases, enhanced breaking in shallow waters produced lower nearshore wave heights (0.5–1.0 m) and distinct circulation cells, whereas high tide allowed greater wave penetration (0.7–1.2 m) with reduced steepness and breaking. Current fields displayed well-developed rip currents during low tide (0.5–1.0 m/s) with clear feeder and return flow structures controlled by bathymetry. At high tide, currents became mainly longshore with weaker rip activity (0.3–0.7 m/s), indicating reduced cross-shore exchange.

The spatial distribution of water levels and currents highlights the influence of wave setup on nearshore circulation. During low tide, Zs (0.3–0.6 m) showed strong alongshore variability, with lower setup near rip necks and elevated setup in adjacent regions, inducing cross-shore pressure gradients that generated offshore-directed rips up to 1.0 m/s. At high tide, Zs was more uniform (1.5–1.8 m), reducing setup gradients and rip intensity. These results confirm that tidal phase and wave setup jointly control rip strength and organization, with low tide favouring stronger, well-defined rips through enhanced setup gradients.

Simulations for August 21 and January 15, 2018, were also conducted but are not presented here. The August run, representing peak monsoon conditions, revealed high wave energy and an expanded surf zone, with rhythmic bar-channel patterns and persistent rips across all tidal phases. Wave heights exceeded 2.5 m, and nearshore circulation was dominated by wide feeder zones merging into seaward-directed jets (>1.5 m/s), reflecting a dynamic balance between wave energy and bathymetric control, resulting in an energetic surf zone. In contrast, the January simulation, representing calm winter conditions, exhibited a dissipative nearshore state with weak hydrodynamics. SWH remained below 0.6 m, the surf zone was narrow with minimal setup gradients, and currents were weak (<0.3 m/s) and diffuse, showing no organized rip circulation, indicating uniform energy dissipation under low wave forcing. The four simulations clearly reveal the seasonal modulation of nearshore hydrodynamics. August and May represent energetic states with stronger wave forcing and active rip currents, followed by October showing comparatively weaker but still noticeable rip activity, whereas January depicts a quiescent winter period with reduced wave energy and minimal rip activity. These findings emphasize the strong dependence of rip current formation and intensity on tidal phase and wave forcing, providing key insight into seasonal morphodynamic variability under varying hydrodynamic regimes and their implications for coastal safety.

3.2. *Analysis of field, satellite, and beach morphodynamics:*

Field and satellite observations (Fig. 6) collectively illustrate the rip current dynamics at the study site through drifter deployments, Sentinel-2 imagery, Rhodamine B dye experiments, and derived beach morphodynamic states. Drifters with an accuracy of 0.02 m/s (Surisetty et al., 2020) were deployed on 15 May and 25 October 2018 (Fig. 6e-f), recording offshore-directed velocities up to 1.2 m/s and 1.0 m/s, respectively. Their trajectories delineate narrow, well-defined exit channels, confirming strong seaward-directed flows associated with rip currents.

Sentinel-2 imagery acquired at times close to the field observations and the four simulation periods, 8 May, 18 January, 21 August, and 20 October 2018, distinctly shows rip channels, sandbars, and other morphodynamic features within the study stretch. These features correspond well with the observed field conditions, indicating significant rip activity. The Rhodamine B dye experiments, conducted concurrently with the drifter deployments, visually confirmed these rip channels. The dye released at identified rip zones dispersed rapidly seaward, forming elongated offshore plumes that matched the drifter trajectories, thereby providing a clear depiction of the rip current structure and strength.

Beach morphodynamic conditions and corresponding rip current likelihood for the four simulation periods further support these observations. The computed dimensionless fall velocity (Ω) ranged from 1.28 to 7.09, representing intermediate to dissipative states (Table 3). The LTT ($\Omega \approx 1.39$) on 15 May, RBB ($\Omega \approx 3.01$) on 21 August, and LTT ($\Omega \approx 1.28$) on 25 October 2018 indicate rip-favourable intermediate to transitional states, whereas the dissipative state ($\Omega \approx 7.09$) on 15 January 2018 corresponds to low-energy surf conditions with minimal rip activity, consistent with earlier studies (Sridevi et al., 2019; Surisetty et al., 2023). These morphodynamic states correspond closely with the features visible in the satellite images (Fig. 6a-d), showing bar-trough formations and rip channels during active months (May, August, and October) and uniform breakers during January. The combined evidence from drifter tracks, dye dispersion, and satellite imagery demonstrates the spatial coherence of rip current patterns and their alignment with the prevailing morphodynamic states.

3.3. *Cross-shore current and rip flow analysis along transects*

For a detailed assessment of rip current dynamics, the *u* component of current velocity, representing the cross-shore flow (positive offshore, negative onshore), was analysed along selected alongshore and cross-shore transects, as shown in Fig. 7, to quantify the width and length characteristics of rip currents under pre- and post-monsoon conditions. Three tidal phases (low, high, and low), as detailed earlier, were examined for each case, with shaded bars in the transect plots indicating rip width and offshore extent.

During the pre-monsoon period (15 May 2018), distinct offshore-directed u-velocity peaks were observed along the south-north transect near the Sri Kalimatha Temple (SKT)-Matsya Darshini Museum

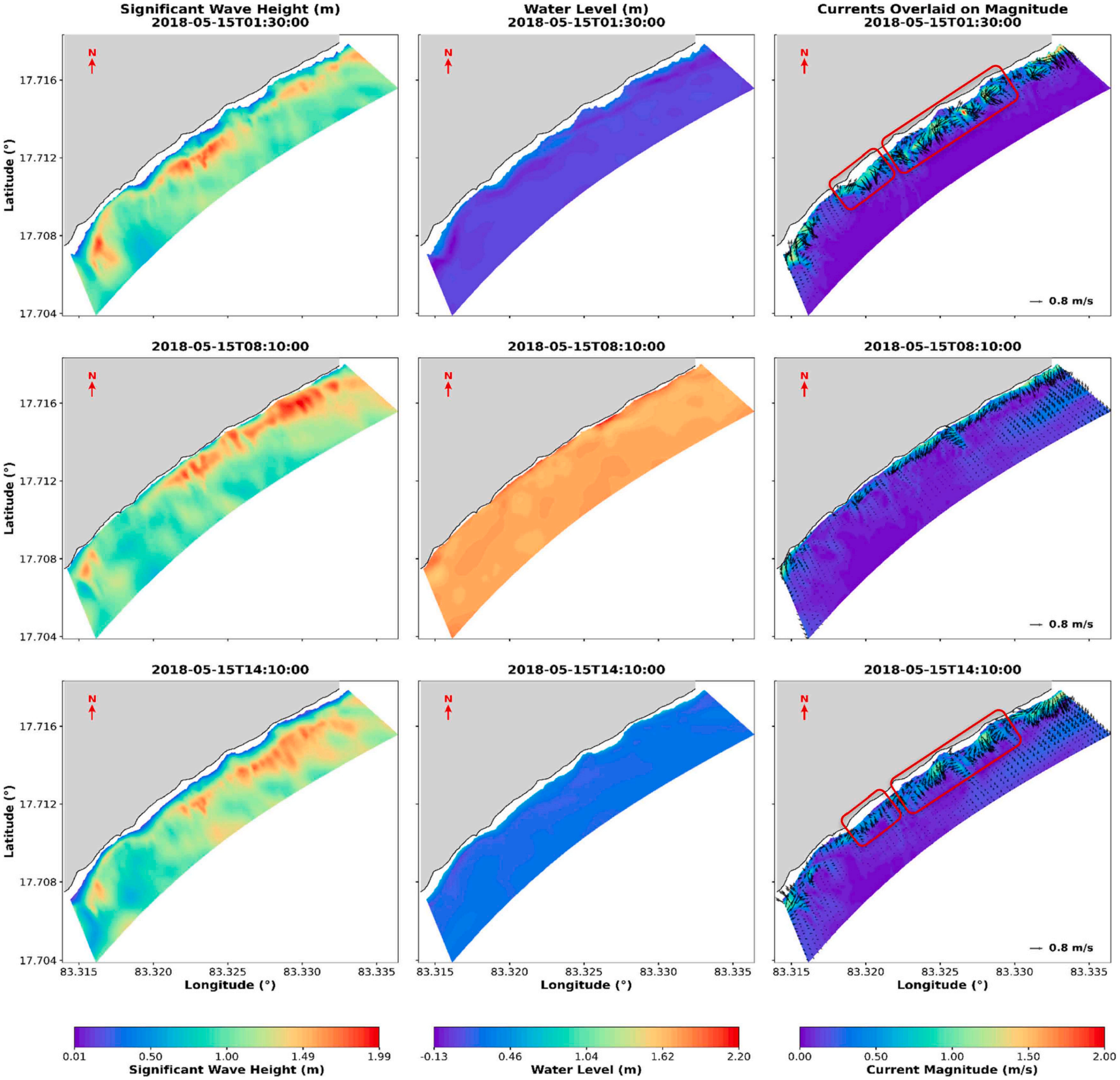

Fig. 4. Spatiotemporal distribution of significant wave height (left), water level (middle), and current velocity vectors overlaid on current magnitude (right) at three different phases: 01:30 (top), 08:10 (middle), and 14:10 IST (bottom) on May 15, 2018. Dotted boxes indicate rip current zones.

(MDM) sector (600–950 m), around the Aqua Sports Complex (ASC) at 1400–2000 m, and north of the Kursura Submarine Museum (KSM) near 2150–2450 m, as illustrated in Fig. 7a. The SKT-MDM stretch exhibited broader rips (15–20 m wide) with relatively weaker offshore currents (0.5 m/s), extending up to about 65 m seaward. Around the AQC, dual rip cells with widths of 14–18 m and higher u values (~1.2 m/s) extended approximately 110 m offshore, indicating stronger, longer rips. The KSM region displayed narrower channels with moderate to high velocities (>0.5 m/s) and an offshore reach of about 75 m. Rip signatures were most distinct during low tide, forming well-defined channels aligned with morphological depressions.

In the post-monsoon case (25 October 2018), as presented in Fig. 7b, offshore-directed flows were less intense and confined within narrower alongshore stretches compared with the pre-monsoon condition. Prominent rips persisted near the MDM, AQC, and KSM, exhibiting a slight northward shift relative to pre-monsoon locations. The MDM site featured moderate widths (14–18 m) with slower currents (<0.5 m/s) and an offshore extent of about 50 m. At the AQC, two active rips with widths of 13–17 m and peak velocities (~1.0 m/s) extended roughly 90 m offshore. North of KSM, the rips were narrower (~60 m long) but remained well-defined.

From the combined alongshore and cross-shore transect analysis, rip currents exhibited a narrow neck nearshore that gradually broadened seaward, forming wider offshore plumes. The AQC region showed the strongest and most persistent rips, with higher velocities and larger offshore extents, whereas the SKT and KSM regions displayed comparatively narrower and shorter rips with gradual offshore decay. Overall, pre-monsoon rips were wider (15–20 m), stronger (up to 1.2 m/s), and longer (65–110 m offshore), whereas post-monsoon rips were narrower (13–18 m), weaker (<1.0 m/s), and shorter (50–90 m offshore). These

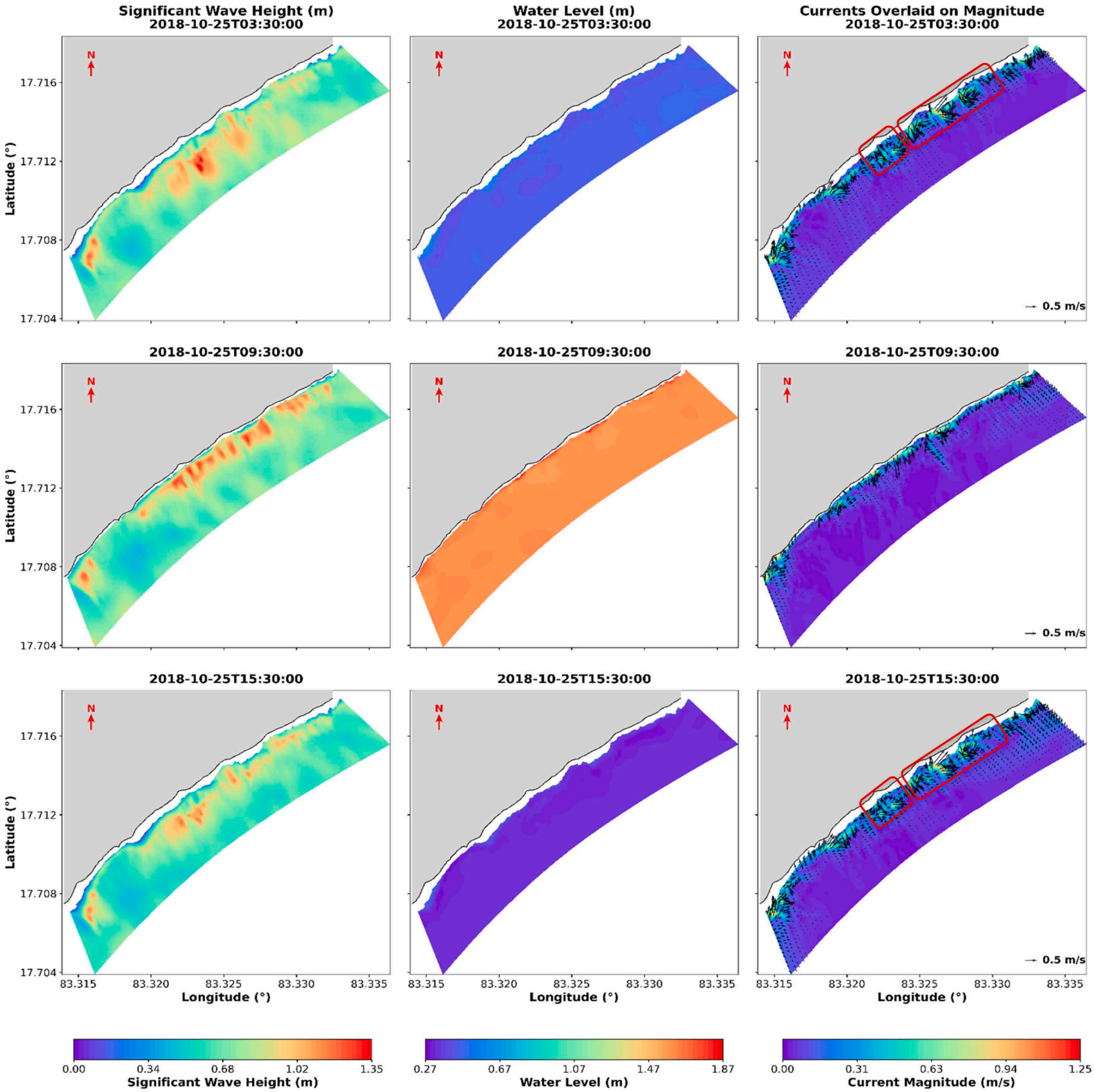

Fig. 5. Spatiotemporal distribution of significant wave height (left), water level (middle), and current velocity vectors overlaid on current magnitude (right) at three different phases: 03:30 (top), 09:30 (middle), and 15:30 IST (bottom) on October 25, 2018. Dotted boxes indicate rip current zones.

patterns reflect seasonal modulation of rip intensity and spatial extent, primarily influenced by nearshore bar realignment and variations in incident wave conditions along the Visakhapatnam coast (Surisetty et al., 2021; Sivaiah B. et al., 2022; Sridevi et al., 2019).

4. Discussions

4.1. Model validation: waves and water levels

Model validation is critical for assessing the accuracy and reliability of numerical simulations. In this study, simulated significant wave height (H), peak wave direction (Dir), water level (WL), and currents were validated against field observations. The model accuracy was quantitatively assessed using the Root Mean Squared Error (RMSE), defined as:

$$\mathrm{RMSE} = \sqrt{\frac{1}{n}\sum_{i=1}^{n}\left(y_{model,i} - y_{obs,i}\right)^2} \tag{12}$$

where $y_{model,i}$ and $y_{obs,i}$ represent the model predicted and observed values at time i, respectively, and n is the total number of observations. A lower RMSE indicates a better agreement between the simulated and observed data. The validation metrics, including RMSE and vector comparisons, provide quantitative and qualitative insights into model performance.

Model performance was examined for four representative periods, 15 January, 15 May, 21 August, and 25 October 2018, corresponding to the northeast (winter), pre-monsoon, southwest (summer) monsoon, and

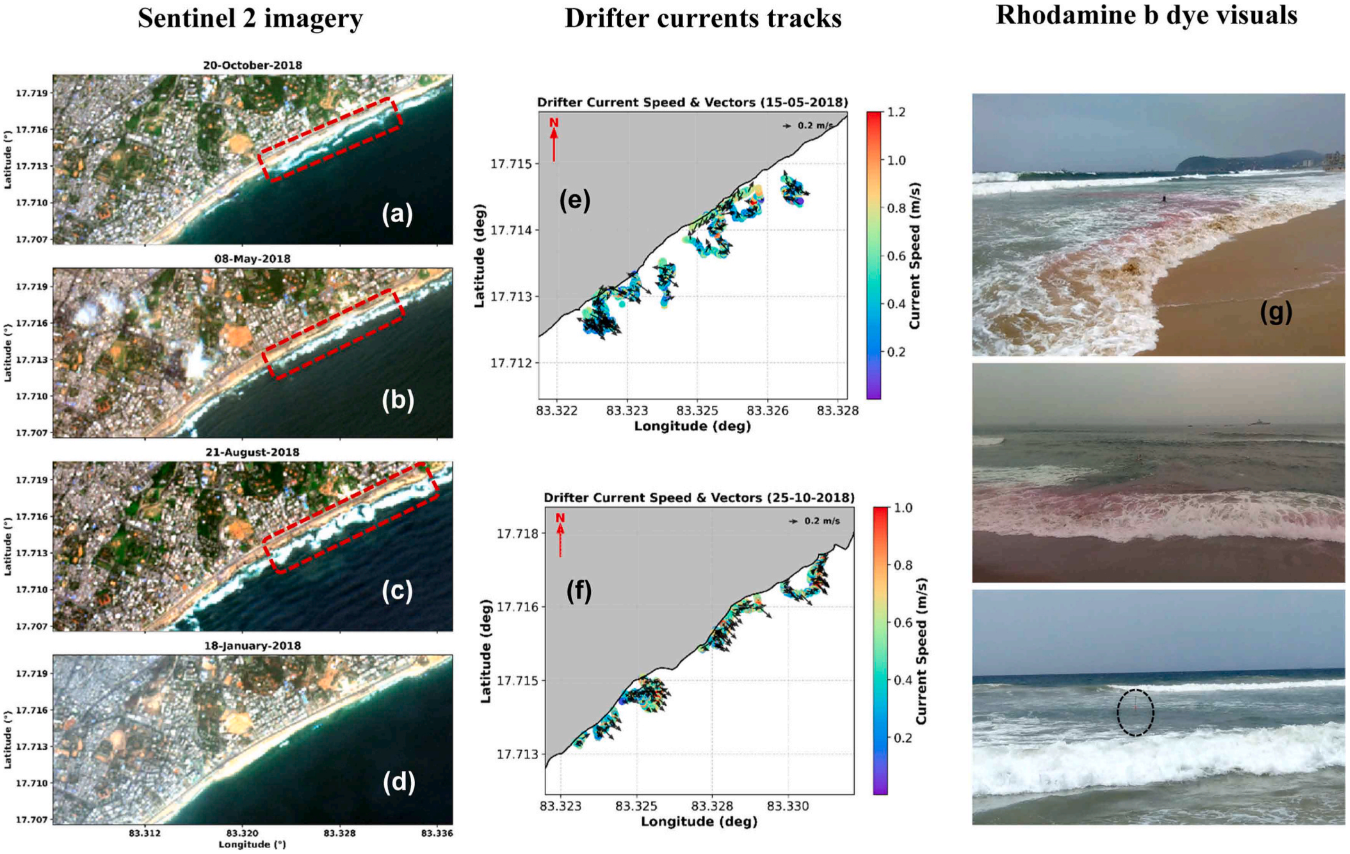

Fig. 6. Field and satellite observations: (a-d) Sentinel-2 imagery showing seasonal nearshore and morphological conditions on 8 May, 18 January, 21 August, and 20 October 2018, corresponding to field measurement and model simulation periods; (e-f) drifter tracks on 15 May and 25 October 2018 showing surface current speed and directions; and (g) Rhodamine B dye visuals captured along with drifters, illustrating nearshore flow and rip currents. Red dotted boxes indicate typical sandbars and rip channels.

Table 3
Computed dimensionless fall velocity (Ω), derived beach morphodynamic states, and associated rip current likelihood for the selected periods at the study site.

Date	D_{50} (mm)	H_s (m)	T (s)	Ω	Beach Morphodynamic State	Rip current likelihood
15 Jan 2018	0.15	0.48	10.56	7.09	D	Very low
15 May 2018	0.85	1.15	14.70	1.39	LTT	Moderate
21 Aug 2018	0.66	1.69	9.78	3.01	RBB	High
25 Oct 2018	0.65	0.75	11.10	1.28	LTT	Moderate

post-monsoon seasons (Fig. 8a-d). Observations from a nearby offshore wave rider buoy and tide gauge station were used for validation. These periods capture the year-round hydrodynamic variability, providing a robust assessment of model performance under seasonal conditions. The model effectively captured the temporal evolution of all parameters across all seasons. During the winter phase, calm sea conditions with low wave heights (<1.0 m) and stable wave directions (120°–160°) were accurately represented, with RMSE values of 0.09 m for H, 0.02 m for WL, and 8.5° for Dir. In the pre-monsoon period, slightly energetic conditions with increased wave heights (~1.5 m) and stronger tidal ranges were well captured. The model effectively reproduced tidal oscillations and short-wave bursts, yielding RMSE values of 0.21 m, 0.04 m, and 10.0° for H, WL, and Dir, respectively, demonstrating reliable boundary forcing and bathymetric representation.

During the southwest monsoon, high-energy conditions prevailed, characterized by elevated wave heights (~1.93 m) and broader directional variability. The model skillfully represented these dynamic conditions with RMSE values of 0.21 m, 0.03 m, and 11.9°, though minor overestimations during peaks may reflect localized wind or dissipation effects. In the post-monsoon case, moderate wave conditions and distinct semidiurnal tides were simulated with high fidelity, yielding RMSE values of 0.13 m for H, 0.03 m for WL, and 10.6° for Dir. A constant merged bathymetry was used to isolate seasonal variability, though limited by the lack of seabed changes that could improve RMSE. The model showed strong skill in capturing observed variations in wave height, direction, and tidal oscillations under both calm and energetic conditions. The close match between modelled and observed peaks, with minimal phase lag, confirms reliable boundary conditions and hydrodynamic forcing, demonstrating robustness for operational nearshore simulations and rip-current forecasting.

4.2. *Validation of currents using drifter observations*

Model-simulated currents were compared with drifter-derived surface currents to evaluate model performance in capturing nearshore flow patterns (Fig. 9a-d). Distinct spatial and seasonal variations in rip current structure and strength were evident across the three zones. During 15 May 2018 (pre-monsoon), two dominant rip cells were

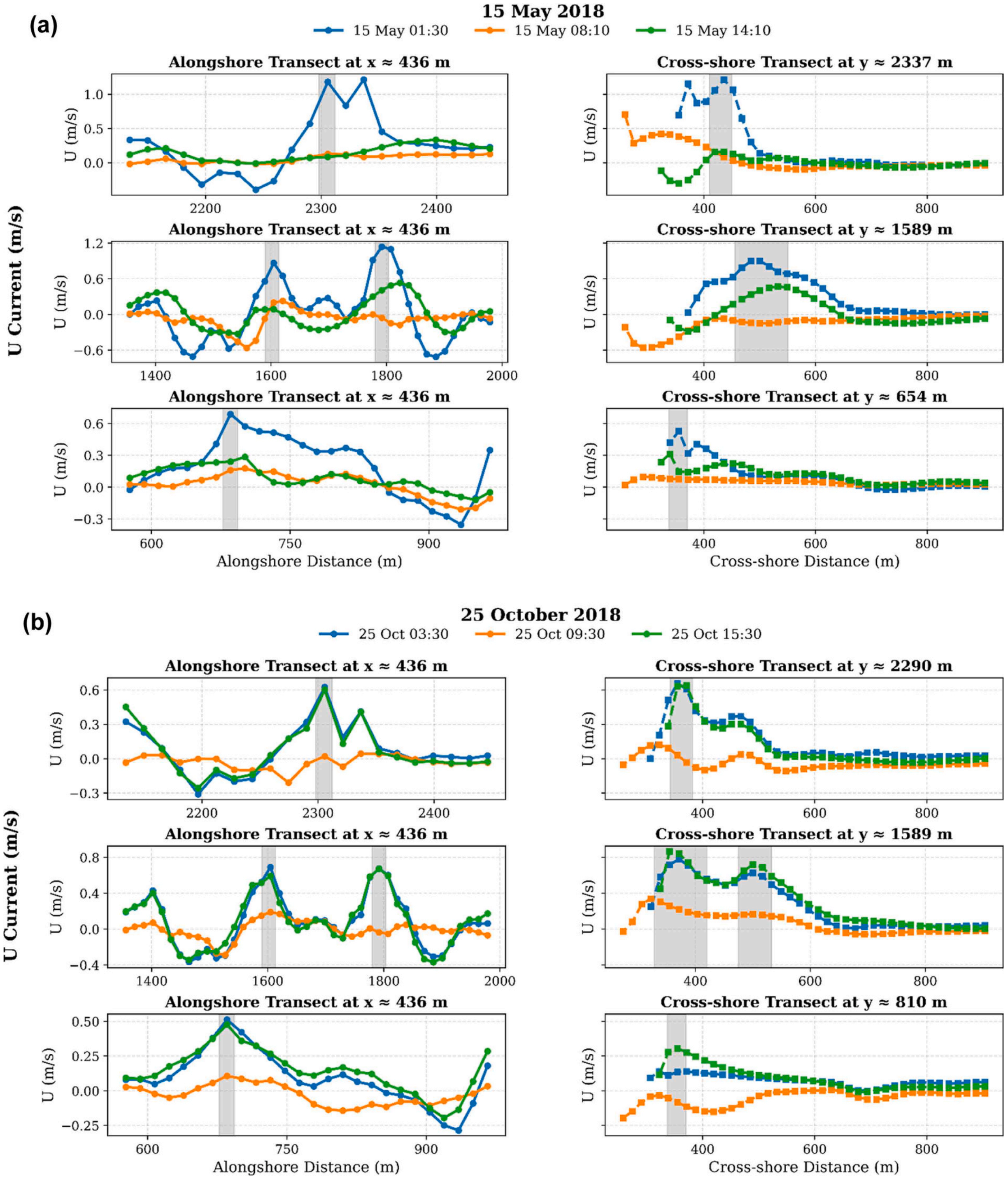

Fig. 7. Alongshore and cross-shore transects of modelled cross-shore current (u) during (a) 15 May 2018 and (b) 25 October 2018, representing pre- and post-monsoon conditions, respectively. Alongshore transects are taken at x ≈ 436 m, and cross-shore transects at y ≈ 654, 1589, and 2337 m for May, and y ≈ 810, 1589, and 2290 m for October. Shaded bars indicate the width and offshore extent of rip currents.

observed slightly south of those in October, depicted in Fig. 9a,b. The southern cell, near the SKT, exhibited an exit-type rip with good agreement between model and drifter currents. The second cell, near MDM, showed a well-defined exit-type rip with larger offshore extent and stronger magnitudes (0.5–1.0 m/s), representing the energetic pre-monsoon environment with south to south-southeast (S-SSE) flow.

During 25 October 2018 (post-monsoon), the rip current zones shifted northward and showed comparatively weaker magnitudes (0.2–0.6 m/s), as shown in Fig. 9c,d. The southern cell, near MDM, remained exit-type (0.5–0.7 m/s) with minor directional and spatial deviations due to localized bathymetric variations. The central cell, near the ASC, also exhibited an exit-type flow (∼0.7 m/s) with strong model-drifter agreement, while the northern cell, near the KSM, displayed a circulatory flow pattern, consistent between model and drifter observations though slightly underestimated in strength. The October currents were primarily southeast to east-southeast (SE-ESE) directed, representing calmer post-monsoon conditions.

The model-simulated vectors appeared smoother than the observed vectors, as localized wind gusts, bathymetric irregularities, short-lived turbulence, and surface flows captured by drifters are typically

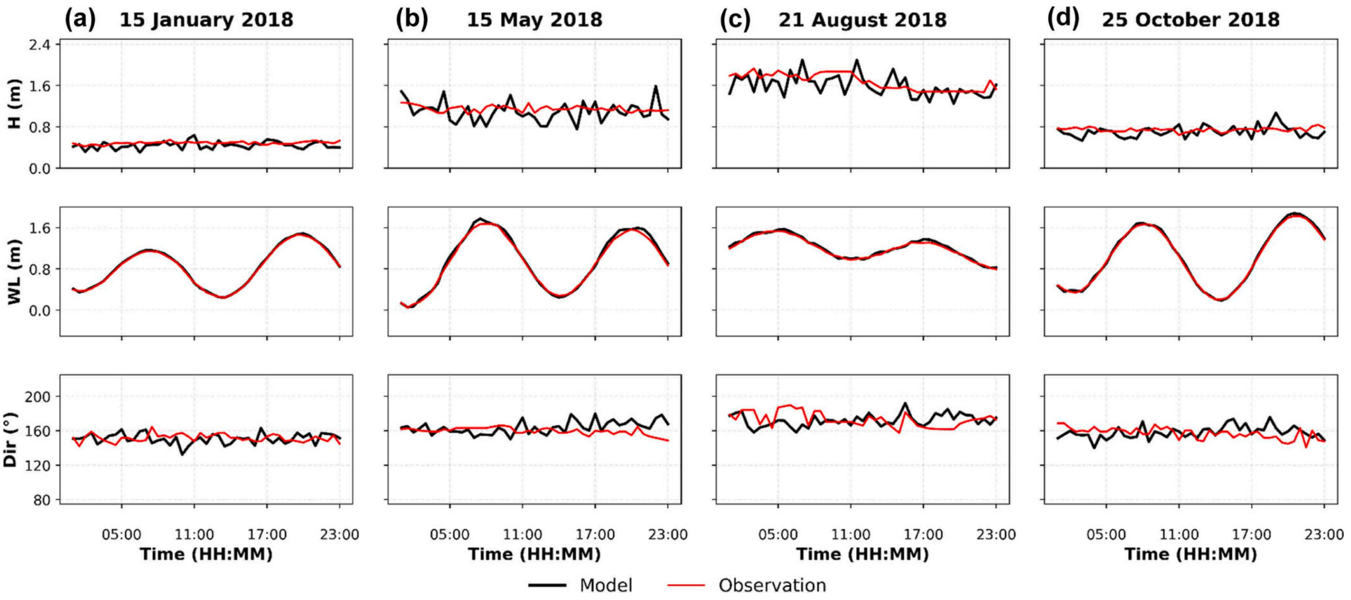

Fig. 8. Time series comparison of model-simulated and observed significant wave height - H (top), water level - WL (middle), and peak wave direction - Dir (bottom) corresponding to (a) 15 January, (b) 15 May, (c) 21 August, and (d) 25 October 2018.

averaged out in the model computations. In the phase-averaged (surfbeat) mode, the model calculates depth-averaged, time-filtered velocities that represent mean circulation patterns, thereby excluding instantaneous variations. In addition, bathymetric smoothing and grid-scale averaging further dampen localized velocity peaks, leading to smoother and more uniform flow fields compared to observations. Nevertheless, current orientations and magnitudes aligned well with drifter observations, supported by RMSE values of 0.15 m/s (May) and 0.16 m/s (October). The agreement between modeled currents, Rhodamine B dye dispersion, and drifter trajectories further confirms the presence of three persistent rip cells, consistent with previous findings (Sivaiah B. et al., 2022; Surisetty et al., 2021; Surisetty et al., 2023). These comparisons confirm that XBeach effectively simulates spatial and seasonal variability of nearshore currents and rip structures, underscoring its reliability for rip current forecasting.

4.3. Bathymetric and morphodynamic control of rip currents

The combined analysis of modelled hydrodynamics (Figs. 4 and 5), morphodynamic states (Table 3), and observed beach configurations (Fig. 6) shows that rip current activity along the study site is mainly governed by the interaction of nearshore bathymetry, tidal stage, and wave forcing. The alongshore transect analysis of bed level (Zb) and cross-shore current (u) profiles (Fig. 10a-c) demonstrates how nearshore morphology regulates cross-shore flow. Transects were selected progressively from the outer surf zone (-4 m) to the inner surf and swash region (-1 m) to examine the influence of bathymetric undulations on u variations. Bar-trough formations become more distinct shoreward (Fig. 3), with corresponding u oscillations marking alternating feeder and rip zones. At x = 597 m (Fig. 10a), pronounced Zb oscillations coincide with peak offshore velocities (~0.6 m/s), defining an active rip neck. At x = 435.7 m (Fig. 10b), alternating bar-trough sequences and strong gradients (up to 1 m/s) represent a well-developed feeder-rip system. Near the beach (x = 338.9 m; Fig. 10c), smoother bed profiles and discontinuous u fields over shallow or exposed areas indicate intermittent flow and weaker offshore currents (<0.8 m/s) under subdued wave forcing. These flow-bed responses reflect the seasonal morphodynamic transitions.

The morphodynamic influence is further supported by the computed Ω values and field conditions. During May, the LTT state with moderate to high waves (Hs ≈ 1.15 m) and coarser sediment (D_{50} = 0.85 mm) enhanced breaker-induced setup gradients, promoting bar development and well-defined rip channels that shifted southward, as evident from the bed undulations in Fig. 10 and the field and satellite observations in Fig. 6a-f. In contrast, the LTT state during October, characterized by finer sediments (D_{50} = 0.65 mm) and lower wave energy (Hs ≈ 0.75 m), produced weaker and northward-shifted rip circulation with reduced offshore extent, consistent with the smoother topography and drifter trajectories shown in Fig. 6a-f. These morphological variations align with the corresponding seasonal beach configurations observed in Sentinel-2 imagery, which depict a low-energy dissipative state in January, rhythmic bar-channel patterns in August, and intermediate LTT conditions in May and October, consistent with the computed Ω values (Sridevi et al., 2019; Surisetty et al., 2023). The correspondence between bathymetric depressions, cross-shore current peaks, and morphodynamic states indicates that rip current strength and position are primarily controlled by bar-channel morphology and wave-tide interactions (Hu et al., 2022; Sun et al., 2025).

5. Conclusions

Nearshore processes, particularly rip currents, are governed by complex interactions among waves, tides, bathymetry, and beach morphology. This study applied the XBeach numerical model in surfbeat mode to simulate wave transformation, water levels, and nearshore circulation along RK Beach, Visakhapatnam, with emphasis on rip current dynamics. The model was forced with high-resolution bathymetry, offshore wave data from a wave rider buoy, and tidal variations from a nearby tide gauge. To represent the year-round hydrodynamic regime, simulations were conducted for January 15, May 15, August 21, and October 25, 2018, corresponding to the northeast, pre-, southwest, and post-monsoon seasons, respectively. These simulations effectively captured the spatial and temporal evolution of rip currents under varying hydrodynamic conditions. Field observations on May 15 and October 25, 2018, including drifter deployments, Rhodamine B dye releases, and Sentinel-2 imagery, were used to validate the simulations. Beach morphodynamic states, derived from wave parameters and sediment grain sizes, were used as proxies for validation where field data were unavailable. Observational wave and water-level data from 2018 were used to represent seasonal hydrodynamic variability in the study site.

Model validation under varying seasonal hydrodynamic conditions

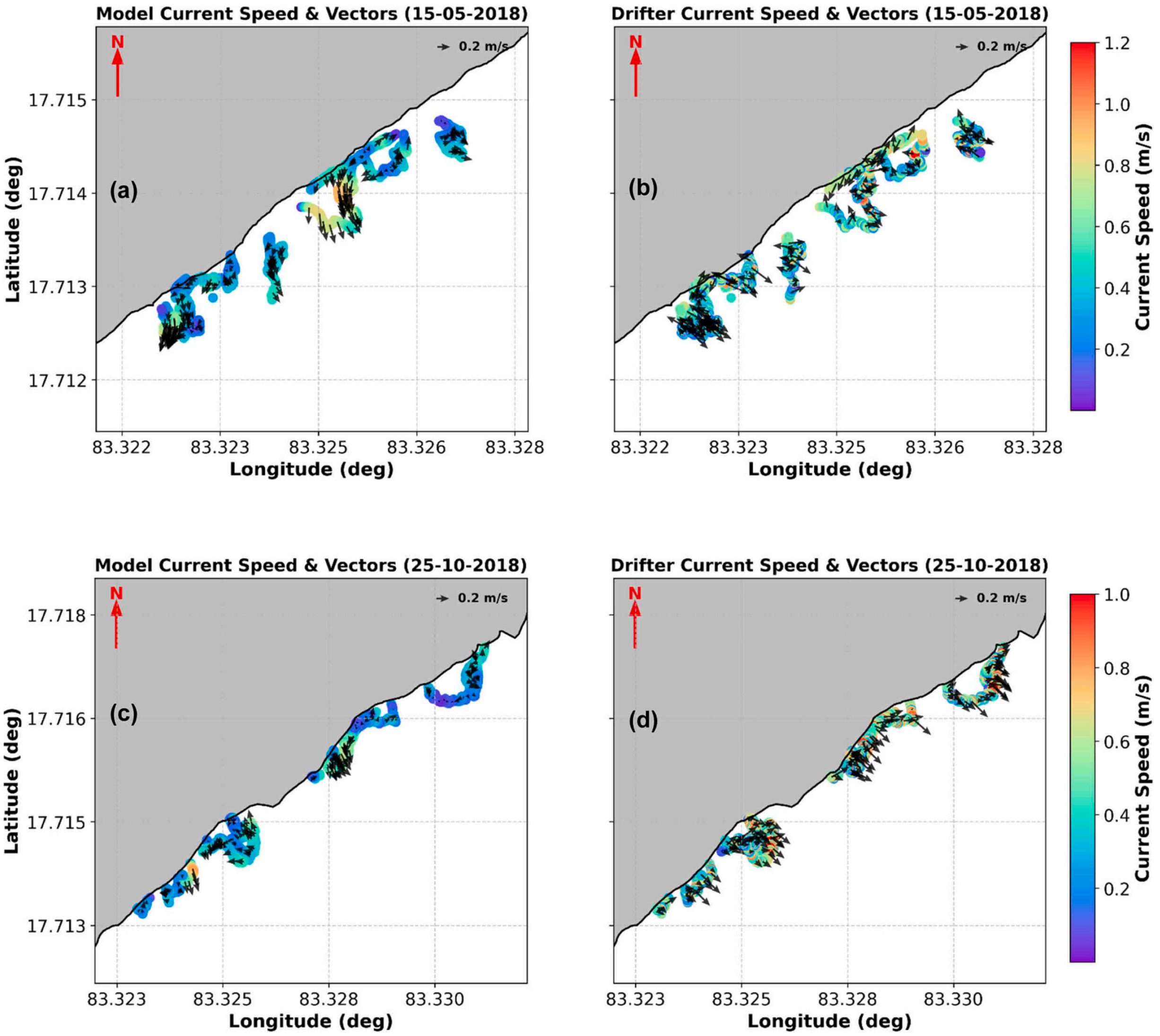

Fig. 9. Comparison of model-simulated (a, c) and drifter-derived (b, d) surface current fields on May 15 (top) and October 25, 2018 (bottom), respectively, showing current magnitudes overlaid with velocity vectors.

showed strong agreement with observations. The model accurately captured wave heights ranging from 0.2 to over 2.5 m and water levels from 0.1 to 1.9 m, achieving RMSE values of 0.09–0.21 m for significant wave height, 0.02–0.04 m for water level, and 8.5°–11.9° for peak wave direction. Simulated current velocities also aligned well with drifter measurements, capturing distinct offshore-directed rip currents of 0.2–1.5 m/s with an overall RMSE of 0.15 m/s across different seasonal regimes. Spatial analysis identified three main rip current zones along RK Beach, SKT-MDM, AQC, and KSM. The AQC showed the strongest and most persistent rips (15–20 m wide, 65–110 m long, 1.0–1.2 m/s), followed by SKT and KSM, especially during low tide when enhanced wave breaking over shallow sandbars intensified offshore flow. These findings highlight the strong tidal control on wave set-up, set-down, and rip current strength. Rhodamine B dye dispersion visually confirmed offshore-directed flow through rip currents, showing strong alignment with both drifter trajectories and model-simulated current vectors. Derived Ω values showed dissipative conditions in January, RBB in August, and LTT in May and October 2018, indicating a shift from low to moderate-high energy states associated with stronger rip activity, consistent with corresponding Sentinel-2 morphological patterns. Sentinel-2 imagery effectively captured rip currents through visible gaps in wave breaking, highlighting sandbar-channel features that aligned well with derived Ω states and model-simulated rip locations, confirming the strong bathymetric and morphodynamic control on rip formation. The seasonal Ω variations, supported by satellite and model outputs, indicated that rip currents were more frequent and intense during the southwest monsoon due to energetic waves and rhythmic bar-trough patterns, moderate during pre- and post-monsoon under enhanced low-tide breaking, and weakest during the northeast monsoon.

While the model effectively simulated seasonal rip dynamics, minor underestimations of peak velocities in high-energy zones indicate the need for improved representation of variable bathymetry, wave, tide, and sediment conditions. Overall, the results show that rip current strength, position, and spatiotemporal variability are primarily governed by wave-tide variability and sandbar-channel morphology. The strong agreement among modelled currents, field observations, derived Ω states, and satellite-derived morphology highlights the capability of XBeach to capture nearshore processes and its potential for developing an operational rip current forecasting framework to issue timely alerts, reduce drownings, enhance coastal safety, and support sustainable tourism.

Declaration of Competing Interest

The authors declare that they have no known competing financial

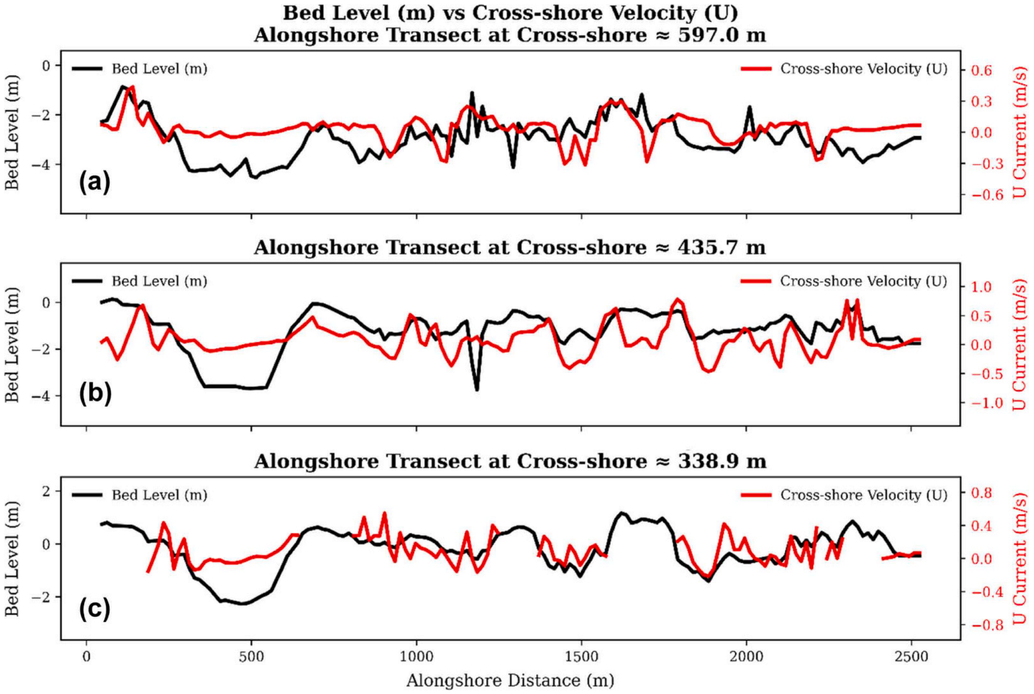

Fig. 10. Variation in bed level (Zb) and cross-shore current (u) profiles for alongshore transects at (a) x = 597 m, (b) x = 435.7 m, and (c) x = 338.9 m on 25 October 2018.

interests or personal relationships that could have appeared to influence the work reported in this paper. We confirm that the work presented in this paper is original and has not been published elsewhere. We also acknowledge the support of our respective institutions and any funding sources that contributed to this research.

Acknowledgements

The authors express their gratitude to the Director of the Indian National Centre for Ocean Information Services (INCOIS) for providing the primary support that enabled this research. The first author thanks Dr. Rashmi Sharma, Deputy Director, Earth, Ocean, Atmosphere, Planetary Sciences Applications Area, SAC ISRO, for leading the SAMUDRA Project and providing essential field data. The authors acknowledge Andhra University for local assistance and support during field activities, the National Institute of Ocean Technology (NIOT) for supplying offshore bathymetry, and the Police Commissioner of Visakhapatnam for granting access to First Information Reports (FIRs) of drowning incidents.

Data availability

Data will be made available on request.

References

Bowen, A.J., Douglas Inman, L., 1969. Rip currents: 2. Laboratory and field observations. J. Geophys Res. 74, 5479–5490. https://doi.org/10.1029/JC074I023P05479.

Brander, R., MacMahan, J.H., 2011. 1 Future challenges for rip current. Rip. Curr. Beach Saf. Phys. Oceanogr. Wave Model.

Brander, R.W., 2015. Rip currents. Coast. Mar. Hazards Risks Disasters 335–379. https://doi.org/10.1016/B978-0-12-396483-0.00012-1.

Caballeria, M., Coco, G., Falqués, A., Huntley, D.A., 2002. Self-organization mechanisms for the formation of nearshore crescentic and transverse sand bars. J. Fluid Mech. 465, 379–410. https://doi.org/10.1017/S002211200200112X.

Casper, A., Nuss, E.S., Baker, C.M., Moulton, M., Dusek, G., 2024. Assessing NOAA rip-current hazard likelihood predictions: comparison with lifeguard observations and parameterizations of bathymetric and transient rip-current types. Weather Forecast 39, 1045–1063. https://doi.org/10.1175/WAF-D-23-0181.1.

Castelle, B., Reniers, A., MacMahan, J., 2014. Bathymetric control of surf zone retention on a rip-channelled beach. Ocean Dyn. 64, 1221–1231. https://doi.org/10.1007/S10236-014-0747-0/FIGURES/9.

Castelle, B., Marieu, V., Bujan, S., Splinter, K.D., Robinet, A., Sénéchal, N., Ferreira, S., 2014. Equilibrium shoreline modelling of a high-energy meso-tidal beach. Mar. Geol. 347, 85–94. https://doi.org/10.1016/j.margeo.2013.11.003.

Castelle, B., Scott, T., Brander, R.W., McCarroll, R.J., 2016. Rip current types, circulation and hazard. Earth Sci. Rev. 163, 1–21. https://doi.org/10.1016/J.EARSCIREV.2016.09.008.

Castelle, Bruno, McCarroll, R.J., Brander, R.W., Scott, T., Dubarbier, B., 2016. Modelling the alongshore variability of optimum rip current escape strategies on a multiple rip-channelled beach. Nat. Hazards 81, 663–686. https://doi.org/10.1007/S11069-015-2101-3/FIGURES/12.

Choi, J., Roh, M., 2021. A laboratory experiment of rip currents between the ends of breaking wave crests. Coast. Eng. 164, 103812. https://doi.org/10.1016/J.COASTALENG.2020.103812.

Dalrymple, R.A., Lozano, C.J., 1978. Wave-current interaction models for rip currents. J. Geophys Res. Oceans 83, 6063–6071. https://doi.org/10.1029/JC083IC12P06063.

Dean, Robert G., Robert, A., 2004. Dalrymple. Coastal processes with engineering applications. Cambridge University Press.

Drozdzewski, D., Shaw, W., Dominey-Howes, D., Brander, R., Walton, T., Gero, A., Sherker, S., Goff, J., Edwick, B., 2012. Surveying rip current survivors: preliminary insights into the experiences of being caught in rip currents. Nat. Hazards Earth Syst. Sci. 12, 1201–1211. https://doi.org/10.5194/NHESS-12-1201-2012.

Drozdzewski, D., Roberts, A., Dominey-Howes, D., Brander, R., 2015. The experiences of weak and non-swimmers caught in rip currents at Australian beaches. Aust. Geogr. 46, 15–32. https://doi.org/10.1080/00049182.2014.953735.

Dudkowska, A., Boruń, A., Malicki, J., Schönhofer, J., Gic-Grusza, G., 2020. Rip currents in the non-tidal surf zone with sandbars: numerical analysis versus field measurements. Oceanologia 62, 291–308. https://doi.org/10.1016/J.OCEANO.2020.02.001.

Ferguson, R.I., Church, M., 2004. A simple universal equation for grain settling velocity. J. Sediment. Res. 74, 933–937. https://doi.org/10.1306/051204740933.

Houser, C., Barrett, G., Labude, D., 2011. Alongshore variation in the rip current hazard at Pensacola Beach, Florida. Nat. Hazards 57, 501–523. https://doi.org/10.1007/S11069-010-9636-0/FIGURES/10.

Hu, Pengpeng, Li, Zhiqiang, Zhu, Daoheng, Zeng, Chunhua, Liu, Run, Chen, Zhaoguang, Su, Qianxin, 2022. Field observation and numerical analysis of rip currents at Ten-Mile Beach, Hailing Island, China. Estuar. Coast. Shelf Sci. 276, 108014.

Ji, Xinran, Xu, Chuanle, Ren, Zhiyuan, Yan, Sheng, Wang, Daoru, Yu, Zongbing, 2023. Study on the formation characteristics and disaster mitigation mechanisms of rip currents on arc-shaped beach. J. Mar. Sci. Eng. 11 (12), 2381.

Ji, Xinran, Wang, Hao, Lu, Xing, Wang, Daoru, Zou, Li, Ren, Zhiyuan, 2025. Hydrodynamic performance of riprap structures in reef lagoon under extreme wave loading: insights from porous media simulations. Phys. Fluids 37 (5).

Ji, Xinran, Meng, Meihua, Huang, Jingtong, Wang, Daoru, Ren, Zhiyuan, 2025. Numerical research on the solitary wave dynamics over coral reefs using a porous media model. Ocean Eng. 341, 122535.

Ji, Xinran, Xu, Chuanle, Ren, Zhiyuan, Wang, Daoru, 2025. Numerical investigation of rip currents near a barred beach induced by irregular waves. Proc. Inst. Mech. Eng. Part M J. Eng. Marit. Environ. 239 (2), 418–434.

Kennedy, A.B., Zhang, Y., 2008. The stability of wave-driven rip current circulation. J. Geophys Res Oceans 113, 3031. https://doi.org/10.1029/2006JC003814.

Komar, Paul D., Gaughan, Michael K., 1973. Airy wave theory and breaker height prediction. Coast. Eng. 1972 405–418.

Kumar, N., Voulgaris, G., Warner, J.C., 2011. Implementation and modification of a three-dimensional radiation stress formulation for surf zone and rip-current applications. Coast. Eng. 58, 1097–1117. https://doi.org/10.1016/J.COASTALENG.2011.06.009.

Kumar, V., Pathak, K., Pednekar, P., Raju, N.S.N., 2006. Coastal processes along the Indian coastline. Curr. Sci. 530–536.

Kumar, V.S., Kumar, K., Ashok, Raju, N.S.N., 2001. Nearshore processes along Tikkavanipalem beach, Visakhapatnam, India. J. Coast. Res. 17, 271–279.

Kumar, V.Sanil, Kumar, K.Ashok, Raju, N.S.N., 2004. Wave characteristics off Visakhapatnam coast during a cyclone. Curr. Sci. 1524–1529.

Lippmann, T.C., Holman, R.A., 1989. Quantification of sand bar morphology: a video technique based on wave dissipation. J. Geophys Res Oceans 94, 995–1011. https://doi.org/10.1029/JC094IC01P00995.

Long, J.W., Özkan-Haller, H.T., 2016. Forcing and variability of nonstationary rip currents. J. Geophys Res. Oceans 121, 520–539. https://doi.org/10.1002/2015JC010990.

Longuet-Higgins, M., Stewart, R.W., 1964. Radiation stresses in water waves; a physical discussion, with applications. Deep Sea Res. Oceanogr. Abstr.

Lushine, J.B., 1991. A study of rip current drownings and related weather factors. Natl. Weather Dig. 16 (3), 13–19.

MacMahan, J.H., Reniers, H.M., Thornton, A.J., Stanton, E.B., T.P, 2004. Surf zone eddies coupled with rip current morphology. J. Geophys. Res. Oceans 109, 7004. https://doi.org/10.1029/2003JC002083.

MacMahan, J.H., Reniers, A.J., Thornton, E.B., Stanton, T.P., 2004. Infragravity rip current pulsations. J. Geophys Res Oceans 109 (C1), C01033. https://doi.org/10.1029/2003JC002068.

MacMahan, J.H., Thornton, E.B., Reniers, A.J.H.M., 2006. Rip current review. Coast. Eng. 53, 191–208. https://doi.org/10.1016/J.COASTALENG.2005.10.009.

Masselink, G., Short, A.D., 1993. The effect of tide range on beach morphodynamics and morphology: a conceptual beach model. J. Coast Res 9, 785–800.

McCarroll, R.J., Castelle, B., Brander, R.W., Scott, T., 2015. Modelling rip current flow and bather escape strategies across a transverse bar and rip channel morphology. Geomorphology 246, 502–518. https://doi.org/10.1016/j.geomorph.2015.06.041.

Panigrahi, J.K., Sathish Kumar, V., Tripathy, J.K., 2010. Littoral drift by alongshore flow at Visakhapatnam – East Coast of India. J. HydroEnviron. Res. 4, 317–327. https://doi.org/10.1016/J.JHER.2010.03.004.

Raju, K.N.P., Vaidyanadhan, R., 1978. Geomorphology of Visakhapatnam, Andhra Pradesh. J. Geol. Soc. India 19, 26–34. https://doi.org/10.17491/JGSI/1978/190103.

Reddy, B.S.R., Sarma, K.G.S., Kumar, K.H., 1984. Beach changes during normal and cyclonic periods along Visakhapatnam coast. Indian J. Mar. Sci. 13 (1), 28–33.

Reniers, A.J.H.M., MacMahan, J.H., Beron-Vera, F.J., Olascoaga, M.J., 2010. Rip-current pulses tied to Lagrangian coherent structures. Geophys. Res. Lett. 37. https://doi.org/10.1029/2009GL041443.

Roelvink, D., Reniers, A., van Dongeren, A., van Thiel de Vries, J., McCall, R., Lescinski, J., 2009. Modelling storm impacts on beaches, dunes and barrier islands. Coast. Eng. 56, 1133–1152. https://doi.org/10.1016/J.COASTALENG.2009.08.006.

Roelvink, D., Reniers, A.J.H.M., Van Dongeren, A.P., Van Thiel de Vries, J., Lescinski, J., McCall, R., 2010. Unesco-IHE institute for water education, deltares and Delft university of technology. XBeach Model Descr. Man.

Sasaki, T.O., Horikawa, K., 1978. Observation of nearshore current and edge waves. Coast. Eng. 791–809. https://doi.org/10.1061/9780872621909.047.

Scott, T., Austin, M., Masselink, G., Russell, P., 2016. Dynamics of rip currents associated with groynes—field measurements, modelling and implications for beach safety. Coast. Eng. 107, 53–69.

Sembiring, L., Van Dongeren, A., Winter, G., Roelvink, D., 2016. Dynamic modelling of rip currents for swimmer safety on a wind-sea–dominated mesotidal beach. J. Coast Res. 32, 339–353. https://doi.org/10.2112/JCOASTRES-D-14-00260.1.

Short, A.D., 2006. Australian beach systems – nature and distribution. J. Coast Res 22, 11–27. https://doi.org/10.2112/05A-0002.1.

Short, A.D., Brander, Robert W., 1999. Regional variations in rip density. J. Coast. Res. 813–822.

Sivaiah, B., Balakrishnan Nair, T.M., Joseph, S., Surisetty, V.V.Arun Kumar, Sridevi, T., Harikumar, R., Srinivas, K., Yatin, G., Gireesh, B., Venkateswararao, K., Venkateswarlu, C., Anjaneyulu, A., Prasad, K.V.S.R., 2022. Identifying rip channels along RK beach, Visakhapatnam using Video and satellite imagery analysis. J. Indian Soc. Remote Sens 50, 1585–1602. https://doi.org/10.1007/S12524-022-01539-2.

Sridevi, T., Surisetty, V.V.Arun Kumar, Kumar, R., 2019. Seasonal variability of rip current probability along a wave-dominated coast using high resolution satellites and wave data. J. Geomat. 13 (1), 149–155.

Suanda, S.H., Feddersen, F., 2015. A self-similar scaling for cross-shelf exchange driven by transient rip currents. Geophys Res. Lett. 42, 5427–5434. https://doi.org/10.1002/2015GL063944.

Sun, Yan, Bian, Xiaodong, Liu, Lulu, Zhu, Daoheng, Li, Zhiqiang, 2025. Comprehensive assessment of the effects of environmental factors on low-energy rip currents. J. Geophys Res. Oceans 130 (4), e2024JC022214.

Surisetty, V.V.Arun Kumar, 2012. Numerical modelling of Coastal and Nearshore processes in the vicinity of Shoreline Harbours with special reference to Visakhapatnam coast, India (Ph.D. Thesis). Andhra University.

Surisetty, V.V.Arun Kumar, Luhar, R.K., Sharma, R., Kumar, R., 2020. Design and development of a low-cost GNSS drifter for rip currents. Curr. Sci. 118 (2), 273–279. https://doi.org/10.18520/cs/v118/i2/273-279.

Surisetty, V.V.Arun Kumar, Prasad, K.V.S.R., 2014. Rip current-related fatalities in India: a new predictive risk scale for forecasting rip currents. Nat. Hazards 70, 313–335. https://doi.org/10.1007/S11069-013-0812-X.

Surisetty, V.V.Arun Kumar, Sivaiah, B., Venkateswarlu, C., Gireesh, B., Sridevi, T., Venkateswara Rao, K., Prasad, K.V.S.R., Sharma, R., 2021. Investigation of rip current processes along Visakhapatnam beaches, east coast of India: a study based on GNSS drifters and dye experiments. J. Earth Syst. Sci. 130, 1–12. https://doi.org/10.1007/S12040-021-01579-1.

Surisetty, V.V.Arun Kumar, Venkateswarlu, C., Ramesh, M., Gireesh, B., Naidu, C.V., Sheela Nair, L., Sharma, R., 2023. Practical use of smartphone cameras in rip current monitoring studies. Ocean Coast Manag. 243, 106776. https://doi.org/10.1016/J.OCECOAMAN.2023.106776.

Vousdoukas, M.I., Almeida, L.P., Ferreira, Ó., 2011. Modelling storm-induced beach morphological change in a meso-tidal environment. Coast. Eng. 58 (8), 892–905. https://doi.org/10.1016/j.coastaleng.2011.05.007.

Wright, L.D., Short, A.D., 1984. Morphodynamic variability of surf zones and beaches: a synthesis. Mar. Geol. 56, 93–118. https://doi.org/10.1016/0025-3227(84)90008-2.

Yu, J., Slinn, D.N., 2003. Effects of wave-current interaction on rip currents. J. Geophys Res Oceans 108, 3088. https://doi.org/10.1029/2001JC001105.

Yuan, Y., Yang, H., Yu, F., Gao, Y., Li, B., Xing, C., 2023. A wave-resolving modeling study of rip current variability, rip hazard, and swimmer escape strategies on an embayed beach. Nat. Hazards Earth Syst. Sci. 23, 3487–3507. https://doi.org/10.5194/NHESS-23-3487-2023.